

# Topological Versatility of Oxalate-Based Bimetallic One-Dimensional (1D) Compounds Associated with Ammonium Cations

Emilio Pardo,<sup>†,§</sup> Cyrille Train,<sup>\*,‡,||</sup> Kamal Boubekeur,<sup>†</sup> Geoffrey Gontard,<sup>†</sup> Joan Cano,<sup>§</sup> Francesc Lloret,<sup>§</sup> Keitaro Nakatani,<sup>⊥</sup> and Michel Verdaguer<sup>\*,†</sup>

<sup>†</sup>Institut Parisien de Chimie Moléculaire, Université Pierre et Marie Curie-Paris 6, UMR CNRS 7201, 75252 Paris cedex 05, France

<sup>‡</sup>Laboratoire National des Champs Magnétiques Intenses, UPR CNRS 3228, Université Joseph Fourier, B.P. 166, 38042 Grenoble cedex 9, France

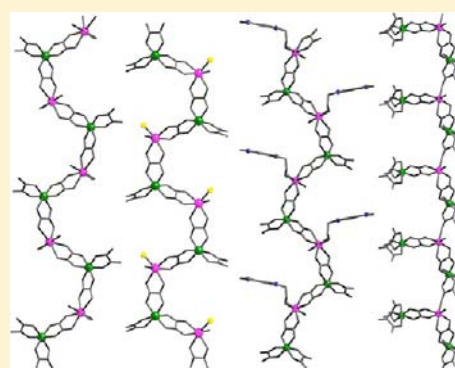
<sup>||</sup>Institut Universitaire de France, 103, bd Saint-Michel 75005 Paris, France

<sup>§</sup>Departament de Química Inorgànica, Instituto de Ciencia Molecular (ICMOL), Universitat de València, 46980 Paterna, València, Spain

<sup>⊥</sup>PPSM (UMR CNRS 8531), Institut d'Alembert (IFR 121, FR 3242), Ecole Normale Supérieure de Cachan, F-94235 Cachan, France

## S Supporting Information

**ABSTRACT:** A new family of oxalate-bridged chains of formula  $(C_1)[Mn(H_2O)_3Cr(ox)_3] \cdot H_2O$  (**1**),  $(C_2)_4[Mn_2(H_2O)_3ClCr_2(ox)_6]Cl \cdot H_2O \cdot 2C_2H_6O$  (**2a**),  $(C_2)_4[Co_2(H_2O)_3ClCr_2(ox)_6]Cl \cdot 2H_2O \cdot 2C_2H_6O$  (**2b**),  $[Mn(C_3)(H_2O)_2Cr(ox)_3] \cdot H_2O$  (**3**), and  $(C_4)_4[Mn(H_2O)\{Cr(\mu-ox)_2\}_2] \cdot H_2O$  (**4**) [ $C_1^+$  = tetramethylammonium,  $C_2^+$  = 4-*N,N*-dimethylaminopyridinium,  $C_3^+$  = 1-hydroxyethyl-4-*N,N*-dimethylamino-pyridinium,  $C_4^+$  = 1-hydroxyethyl-4-(4'-dimethylamino- $\alpha$ -styryl)-pyridinium,  $ox^{2-}$  = oxalate] have been synthesized by self-assembly of the  $(C_n)_3[Cr(ox)_3]$  ( $n = 1-4$ ) mononuclear compound and the chloride salts of the corresponding metal(II) ions. The crystal structures of the five chain compounds have been determined by single-crystal X-ray diffraction. Compounds **1** and **2** crystallize in the *Pc* and *P2<sub>1</sub>/c* centrosymmetrical space groups, respectively, whereas **3** and **4** crystallize in the *C2cb* and *P1* noncentrosymmetrical space groups, respectively. Compounds **1**, **2**, and **3** adopt a zigzag chain structure while **4** exhibits a comb-like chain structure consisting of the repetition of the  $[Mn(H_2O)\{Cr(\mu-ox)(ox)_2\}\{Cr(\mu-ox)_2(ox)\}]^{4-}$  entities. Compound **3** displays large second-order optical nonlinearity. The magnetic properties of **1-4** have been investigated in the temperature range 2–300 K. Monte Carlo simulations on **1**, **2a**, **2b**, and **3** provide a quantitative description of the magnetic properties indicating ferromagnetic interactions through the bis(bidentate) oxalate bridges [ $J = +0.55 \text{ cm}^{-1}$  (**1**),  $J = +1.02 \text{ cm}^{-1}$  (**2a**),  $J = +3.83 \text{ cm}^{-1}$  (**2b**), and  $J = +0.75 \text{ cm}^{-1}$  (**3**) using Hamiltonian  $\hat{H} = -J(\hat{S}_i \cdot \hat{S}_j)$ ]. On the other side, the fit of the magnetic susceptibility data of **4** by full-matrix diagonalization agrees with a ferromagnetic exchange interaction within the  $[Mn(H_2O)\{Cr(\mu-ox)(ox)_2\}\{Cr(\mu-ox)_2(ox)\}]^{4-}$  trinuclear units ( $J = +2.07 \text{ cm}^{-1}$ ) antiferromagnetically coupled along the chain. Compound **2b** exhibits a metamagnetic behavior, the value of the critical field being  $H_C = 1000 \text{ G}$ , due to the occurrence of weak interchain antiferromagnetic interactions.



## INTRODUCTION

Since the pioneering work of Werner on the resolution of tris(oxalato)metalate(III),<sup>1</sup> the oxalato ligand ( $C_2O_4^{2-} = ox$ ) is widely used in coordination chemistry, and a large number of oxalate-based species have been reported with an extended range of magnetic properties.<sup>2</sup> This interest in oxalate ligand is due to the large variety of its coordination modes<sup>3</sup> and to its efficiency to transmit electronic effects between neighboring magnetic centers.<sup>4</sup> Furthermore, the anionic coordination networks  $[M^{II}M^{III}(\mu-ox)_3]^-$  synthesized from molecular precursors such as tris(oxalato)chromate(III) and a divalent transition metal ion present two other advantages: they can exhibit chirality and welcome a wide variety of functional cations. Such a versatility is an open door toward new classes of

hybrid materials and multifunctional molecule-based magnets exhibiting new physical properties.<sup>5</sup> The synthesis and design of new hybrids displaying both magnetic properties and large second-order optical nonlinearities (NLO behavior)<sup>6,7</sup> are of fundamental interest for chemists, physicists, and materials' scientists because second harmonic generation (SHG) and electro-optical (EO) devices are important valuable targets.<sup>8</sup> Insertion of hyperpolarizable guests, such as stilbazolium-type chromophores, in magnetic hosts is obviously a suitable strategy.<sup>9,10</sup>

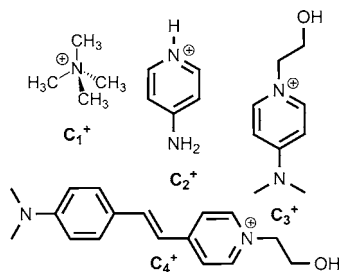
Received: July 10, 2012

Published: October 22, 2012

Two- (2D) and three- (3D) dimensional heterometallic oxalates are well adapted to wrap around templating counterions ( $C^+$ ).<sup>11,12</sup> On the contrary,  $\mu$ -oxalato heterometallic 1D compounds or 0D discrete units are less frequent in this context. To achieve low dimensional systems, blocking ligands substituting one or two oxalate ligands of the building block and/or partially blocking coordination sites of the divalent transition metal ions are efficient<sup>13–16</sup> but not compulsory.<sup>10,17,18</sup>

We question in the present contribution the possibility to force the 1D dimensionality through parameters such as solubility, steric hindrance, and intermolecular interactions. We report the synthesis, the crystal structure, and the optical and magnetic studies of five heterobimetallic oxalate-bridged chains:  $C_1[Mn(H_2O)_3Cr(ox)_3] \cdot H_2O$  ( $C_1^+$  = tetramethylammonium; ox = oxalate) (**1**),  $(C_2)_4[M_2(H_2O)_3ClCr_2(ox)_6] \cdot Cl \cdot nH_2O \cdot 2C_2H_6O$  [ $C_2^+$  = 4-*N,N*-dimethylaminopyridinium; M = Mn,  $n = 1$  (**2a**), M = Co,  $n = 2$  (**2b**)],  $[Mn(C_3)(H_2O)_2Cr(ox)_3] \cdot H_2O$  (**3**) ( $C_3^+$  = 1-hydroxyethyl-4-*N,N*-dimethylamino-pyridinium), and  $(C_4)_4[Mn(H_2O)\{Cr(ox)_3\}_2] \cdot H_2O$  (**4**) ( $C_4^+$  = 1-hydroxyethyl-4-(4'-dimethylamino- $\alpha$ -styryl)-pyridinium) (Scheme 1). We discuss the parameters that influence their final architecture and their magnetic behavior.

Scheme 1. Organic Cations.



## EXPERIMENTAL SECTION

The details of the synthesis are given in the Supporting Information including the synthetic scheme for  $C_4I$  (Scheme S1).

**Physical Techniques.** Elemental analyses (C, H, N) were performed by the Service Interdisciplinaire d'Aide à la Recherche et à l'Enseignement (S.I.A.R.E.) of UPMC Paris (France). IR spectra were recorded on a Perkin-Elmer 882 spectrophotometer as KBr pellets. The second harmonic generation (SHG) was measured by the Kurtz-Perry powder technique.<sup>19</sup> By focusing the 1064 nm fundamental of a Nd:YAG nanosecond laser in a 40 atm  $H_2$  cell, the 1907 nm beam was generated (Raman effect). This IR beam was focused on microcrystalline powder samples. The generated second harmonic was selected through appropriate filters, detected by a photomultiplier, and the signal was recorded on an ultrafast oscilloscope. The powder samples were put between two glass plates and not calibrated. Calibrated urea powder (80–125  $m\mu$ ) served as reference. Magnetic measurements were carried out on powdered samples (from single crystals) of **1–4** with a Quantum Design SQUID magnetometer. Variable-temperature (1.8–300 K) direct current (dc) magnetic susceptibility was measured under applied magnetic fields of 1 T ( $T > 30$  K) and 0.01 T ( $T \leq 30$  K). For **2b**, it was further measured between 2 and 10 K for applied magnetic fields between 0.05 and 0.15 T. The alternating current (ac) magnetic susceptibility of **2b** was measured at  $T = 2.0$  K with a frequency of 100 Hz. The susceptibility data were corrected for the diamagnetism of the constituent atoms and the sample holder.

**Crystal Structure Data Collection and Refinement.** X-ray diffraction data on single crystals of **1–4** were collected on a Nonius Kappa CCD diffractometer. Crystal parameters and refinement results are summarized in Table 1. Data collection and data reduction were done with the COLLECT and EVALCCD programs.<sup>20</sup> Empirical absorption corrections were carried out using SADABS.<sup>21</sup> The structures were solved by direct methods and refined with full-matrix least-squares technique on  $F^2$  using the SHELXS-97 and SHELXL-97 programs.<sup>22</sup> within the WINGX interface.<sup>23</sup> The final geometrical calculations and the graphical manipulations were carried out with PARST97 and CRYSTALMAKER programs, respectively.<sup>24</sup> Main bond lengths and angles for **1–4** are listed in Tables S3–S7. Crystallographic data (excluding structure factors) for the structure reported in this paper have been deposited at the Cambridge Crystallographic Data Centre as CCDC-869842 (**1**), CCDC-869843 (**2a**), CCDC-869844 (**2b**), CCDC-869845 (**3**), and CCDC-869846

Table 1. Summary of Crystallographic Data for **1–4**

	1	2a	2b	3	4
formula	$C_{10}H_{20}CrMnNO_{16}$	$C_{44}H_{64}Cl_2Cr_2Mn_2N_8O_{30}$	$C_{44}H_{66}Cl_2Cr_2Co_2N_8O_{31}$	$C_{15}H_{19}CrMnN_2O_{15}$	$C_{80}H_{88}Cr_2MnN_8O_{30}$
$M$ (g mol <sup>-1</sup> )	517	1470	1496	574	1800
crystal system	monoclinic	monoclinic	monoclinic	orthorhombic	triclinic
space group	$Pc$	$P2_1/c$	$P2_1/c$	$C2cb$	$P1$
$a$ (Å)	9.3746(11)	21.239(4)	10.7446(17)	11.2670(16)	10.5240(10)
$b$ (Å)	11.9158(17)	15.109(2)	14.9493(15)	17.750(4)	12.8130(10)
$c$ (Å)	10.2291(9)	21.809(3)	21.948(3)	23.321(2)	15.440(2)
$\alpha$ (°)	90.00	90.00	90.00	90.00	91.666(12)
$\beta$ (°)	115.202(10)	115.163(9)	116.322(9)	90.00	94.199(7)
$\gamma$ (°)	90.00	90.00	90.00	90.00	90.373(10)
$V$ (Å <sup>3</sup> )	1033.9(2)	6334.0(18)	3159.8(7)	4663.9(12)	2075.4(4)
$Z$	2	4	2	8	1
$\rho_{calc}$ (g cm <sup>-3</sup> )	1.661	1.541	1.566	1.627	1.441
$F(000)$	528	3024	1528	2312	937
$\mu$ (mm <sup>-1</sup> )	1.212	0.899	1.028	1.082	0.496
$T$ (K)	200(1)	200(2)	200(2)	200(2)	200(2)
$R^a$ [ $I > 2\sigma(I)$ ] (all)	0.0400 (0.0660)	0.0609 (0.1223)	0.0543 (0.1002)	0.0430 (0.0779)	0.0529 (0.1325)
$wR^b$ [ $I > 2\sigma(I)$ ]	0.0810 (0.0888)	0.1612 (0.2123)	0.1338 (0.1537)	0.0939 (0.1065)	0.0773 (0.0942)
$S^c$ (all)	0.986	1.030	1.080	0.945	1.006

$$^aR = \sum(|F_o| - |F_c|) / \sum|F_o|, \quad ^b wR = [\sum w(|F_o| - |F_c|)^2 / \sum w|F_o|^2]^{1/2}, \quad ^c S = [\sum w(|F_o| - |F_c|)^2 / (N_o - N_p)]^{1/2}.$$

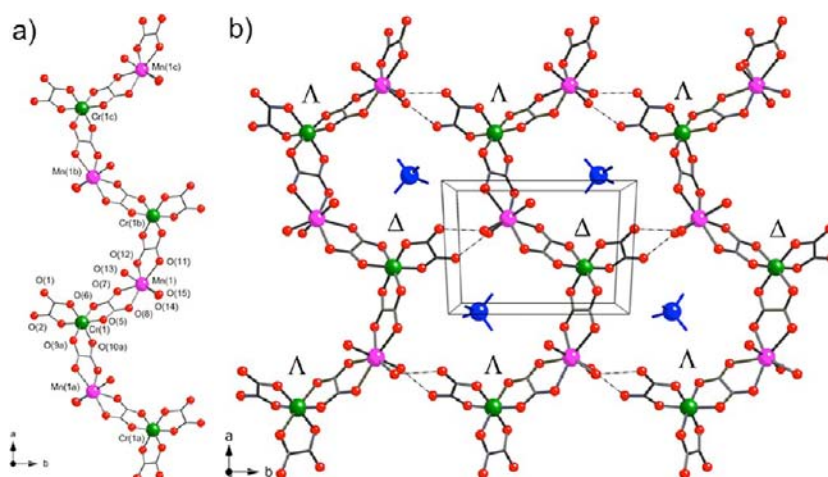


**Figure 1.** Compound 1. (a) View of the  $[\text{Cr}(\text{ox})_3\text{Mn}(\text{H}_2\text{O})_3]^-$  heterobimetallic unit showing the atom numbering. (b) Crystal packing of the chains in the  $ab$  plane in balls and sticks representation, the balls being green for Cr, purple for Mn, and red for O. Nitrogen atoms (in tetramethylammonium cations) are represented in blue. Hydrogen atoms and free water molecules are omitted for clarity. The dotted lines represent hydrogen bonds. [Symmetry codes: (a) =  $x - 1, -y + 1, z - 1/2$ ; (b) =  $x + 1, -y + 1, z + 1/2$ ; (c) =  $x + 2, y, z + 1$ ].

(4). Copies of the data can be obtained free of charge on application to CCDC, 12 Union Road, Cambridge CB21EZ, UK (fax: (+44) 1223-336-033; e-mail: deposit@ccdc.cam.ac.uk).

**Computational Details.** Quantum Monte Carlo (QMC) simulations were carried out for compounds 1, 2, and 3 by using the decoupled cell method, where the probability of a spin flip is calculated from the exact solution of a model that is made up of the spin under consideration and of its first and second neighbors.<sup>25</sup> The one-dimensional model was built by repeating a cell with 7 sites to reach a total number of centers close to 100. Moreover, periodic boundary conditions were imposed. The number of Monte Carlo steps per site at each temperature was fifty thousand, and one tenth was used in the thermalization process. Finally, the  $\chi_M T$  product was evaluated from the magnetization fluctuation. From the results obtained by following this strategy, we have procured empirical laws which allow the simulation of the empirical data and that relate the  $\chi_M T$  product with the reduced temperature,  $T_r = T/J$ , where  $J$  is the exchange magnetic coupling expressed in kelvins. The empirical laws used to reproduce the temperature dependence of the magnetic susceptibility for regular chromium(III)–manganese(II) and chromium(III)–cobalt(II) 1D models were obtained by minimizing a quotient between two polynomials through eq 1:

$$\chi_M T = g_a^2 \frac{\sum_{i=0}^5 B_i (1 + A_i \alpha^2) T_r^i}{\sum_{i=0}^5 D_i (1 + C_i \alpha^2) T_r^i} \quad (1)$$

where  $\chi_M$  is the molar magnetic susceptibility per  $[\text{MnCr}]$  and  $[\text{CoCr}]$  unit, respectively, and  $\alpha$  is the ratio between the Zeeman factors of the  $\text{M}^{\text{II}}$  [ $\text{M} = \text{Mn}^{\text{II}}$  ( $S = 5/2$ ) and  $\text{Co}^{\text{II}}$  ( $S = 3/2$ )] and  $\text{Cr}^{\text{III}}$  ( $S = 3/2$ ) ions ( $\alpha = g_M/g_{\text{Cr}}$ ). The polynomial coefficients from eq 1 for the  $[\text{MnCr}]$  and  $[\text{CoCr}]$  chains are listed in Tables S8 and S9, respectively.  $F$  is the agreement factor defined as  $F = \sum [(\chi_M T)_{\text{exp}} - (\chi_M T)_{\text{calcd}}]^2 / \sum [(\chi_M T)_{\text{exp}}]^2$ .

## RESULTS

**Description of the Structures.** The crystal structures of the five chain compounds reported in this manuscript share a similar six-coordinate environment for the Cr(III) ions which are surrounded by three bidentate oxalate ligands forming a slightly distorted octahedron in an approximate  $D_3$  environment [ $\text{Cr}-\text{O} = 1.95\text{--}2.01 \text{ \AA}$ ] (Tables S3–S7).

$(\text{C}_1)[\text{Mn}(\text{H}_2\text{O})_3\text{Cr}(\text{ox})_3] \cdot \text{H}_2\text{O}$  (1). Compound 1 consists of anionic oxalate-bridged manganese(II)–chromium(III) zigzag chains running along the  $[102]$  direction (Figure 1; Table S3).

Each  $\text{Mn}(\text{H}_2\text{O})_3\text{Cr}(\text{ox})_3$  unit ( $\text{Mn}-\text{Cr}$ ) bears one negative charge. One tetramethylammonium cation per  $\text{Mn}-\text{Cr}$  unit insures the electroneutrality. Within each chain, the tris(oxalato)chromate(III) moiety acts as bis(bidentate) ligand through the carbonyl oxygen atoms of two oxalate groups toward the manganese(II) units (Figure 1a). Three coordinated water molecules complete the coordination sphere of the manganese(II) ion leading to a hepta-coordinated  $[\text{MnO}_7]$  distorted pentagonal bipyramid (Figure 1a) [ $\text{Mn}-\text{O} = 2.314(2)\text{--}2.430(2) \text{ \AA}$  and  $\text{Mn}-\text{O}(\text{w}) = 2.119(3)\text{--}2.223(2) \text{ \AA}$ ]. The absolute configurations ( $\Delta$  and  $\Lambda$ ) of the Cr(III) centers alternate regularly along the chain leading to achiral zigzag chains (Figure 1b).

In the crystal lattice, the chains are quite close to each other in the  $ab$  plane (Figures 1b and 2). The shortest interchain

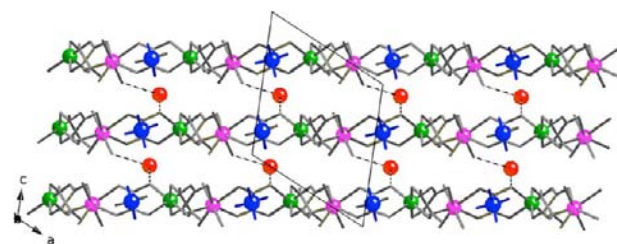


**Figure 2.** Compound 1: Crystal packing of the chains in the  $ac$  planes. Same representation code as in Figure 1. Crystallization water molecules are highlighted in red.

$\text{Cr}^{\text{III}}\text{--Cr}$ ,  $\text{Mn}^{\text{II}}\text{--Mn}$  and  $\text{Cr}^{\text{III}}\text{--Mn}$  distances are 7.6079(10), 6.4222(9), and 5.9644(10)  $\text{ \AA}$ , respectively, whereas the  $\text{Cr}^{\text{III}}\text{--Mn}$  distances within the chain are in the 5.6096(10)–5.6488(9)  $\text{ \AA}$  range. Hydrogen bonds exist between two of the coordinated water molecules and carbonyl oxygen atoms of the adjacent chain [ $\text{O}^{\text{II}}\text{--O}(\text{w}) = 2.6701(37)\text{--}2.8076(34) \text{ \AA}$ ] and build a honeycomb two-dimensional (2D) supramolecular motif combining hydrogen and coordination bonds in the  $ab$  plane (Figure 1b). The centers of these hexagonal cells are occupied by the  $\text{NMe}_4^+$  cations. The crystallization water molecules are located between these planes creating a repeating pattern down the  $c$  axis (Figure 2). They establish hydrogen bonds [ $\text{O}^{\text{II}}\text{--O}(\text{w}) = 2.7795(70)\text{--}2.8239(69) \text{ \AA}$ ] with the oxygen



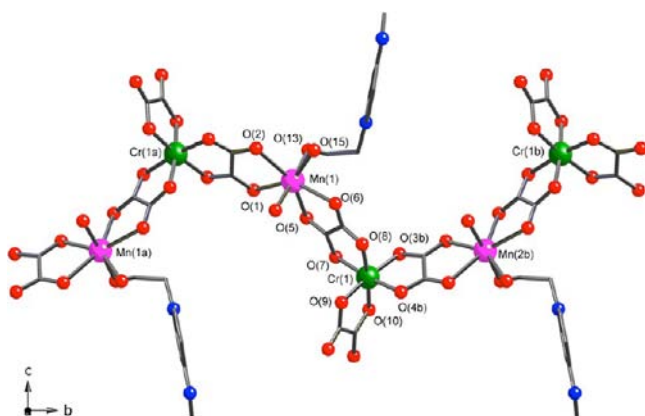


**Figure 5.** Compound 3: View of a fragment of a chain with the atom numbering. Same representation code as in Figure 1 [Symmetry codes: (a) =  $x, y - 1/2, -z + 1/2$ ; (b) =  $x, y + 1/2, -z + 1/2$ ].

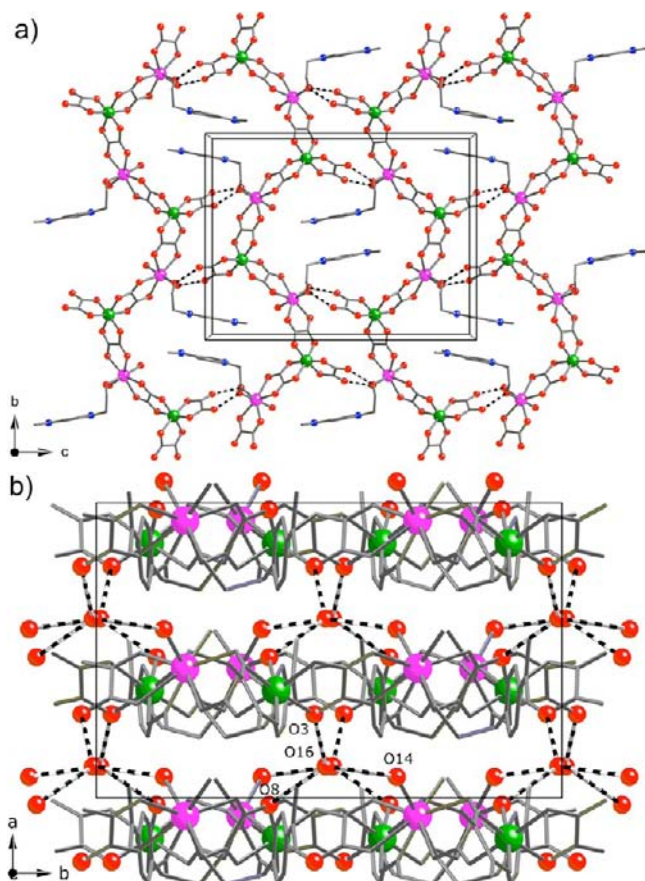


**Figure 6.** Compound 3: Crystal packing of the chains in the  $bc$  (a) and  $ab$  (b) planes, respectively. Same representation code as in Figure 1.

configurations of the Cr(III) centers alternate regularly along the chain leading to achiral zigzag chains (Figure 5).

The packing of the neutral chains in the  $bc$  plane is shown in Figure 6a. In the planes, the neighboring chains are close to each other. The shortest interchain  $\text{Cr}^{\text{III}}\text{--Cr}^{\text{III}}$ ,  $\text{Mn}^{\text{II}}\text{--Mn}^{\text{II}}$ , and  $\text{Cr}^{\text{III}}\text{--Mn}^{\text{II}}$  distances are 7.2264(9), 6.4902(9), and 7.3864 Å, respectively, whereas the  $\text{Cr}^{\text{III}}\text{--Mn}^{\text{II}}$  distances in the chain are in the range 5.6105(13) and 5.7095(8) Å. The coordinated water molecules are connected to the carbonyl oxygen atoms of the adjacent chains by means of hydrogen bond interactions [ $\text{O}^{\text{--}}\text{O}(\text{w}) = 2.6701(37)\text{--}2.8076(34)$  Å] paving the  $bc$  plane by

two types of diamond-shaped bimetallic motifs (Figure 6a). The bigger diamond-shaped cells are occupied by two  $\pi$ -stacked cations [closest contact between the aromatic rings of 3.5407(48) Å] leading to a 2D supramolecular motif combining coordination bonds, hydrogen bonds, and  $\pi$ - $\pi$  interactions (Figure 6a). The neutral chains form layers perpendicular to  $a$ , with crystallization water molecules located between the planes (Figure 6b). The crystallization water molecules establish hydrogen bonds with the carbonyl oxygen atoms of the oxalate groups on one side and with a coordinated water molecule of the adjacent A layer on the other side [ $\text{O}(\text{w})^{\text{--}}\text{O}(\text{w}) = 2.7405(33)\text{--}2.8463(37)$  Å] (Figure 6b). Finally, the coordinated polar cations are stacked in the  $[010]$  direction (Figure 7) with a resulting net dipolar moment aligned along the  $a$  axis.

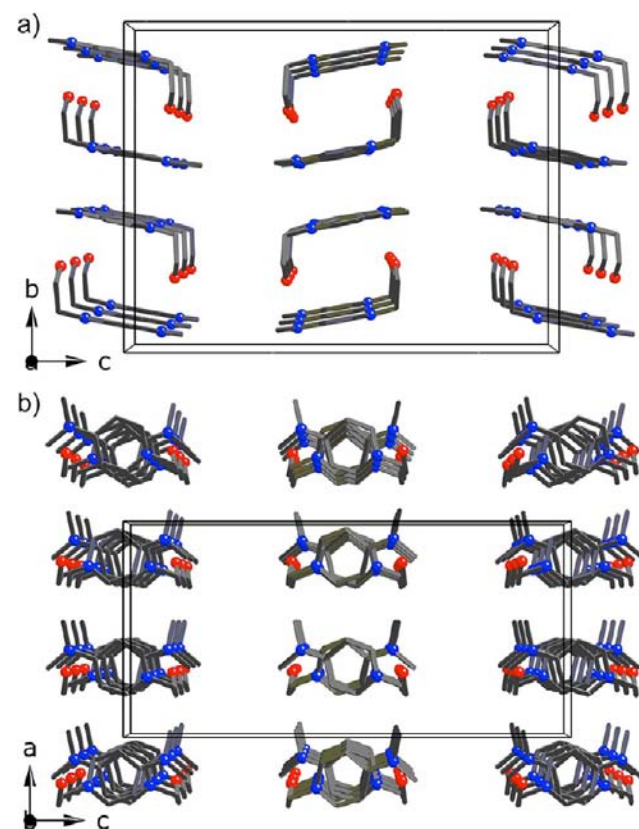


**Figure 7.** Compound 3: Crystal packing of the 4-*N,N*-dimethylamino-1-hydroxyethylpyridinium polar cations in the  $bc$  (a) and  $ac$  (b) planes, emphasizing the polar arrangement of the guest molecules. Same representation code as in Figure 1.

Along the columns, the cations are related to one another by a  $140^\circ$  rotation around the  $b$  axis (Figure 7b). The non-cancellation of the dipolar moment at the crystal level, in the non-centrosymmetric  $C2cb$  space group, opens the possibility to observe optical nonlinearity.

$(C_4)_4[Mn(H_2O)\{Cr(ox)_3\}_2] \cdot H_2O$  (4). Compound 4 consists of oxalate-bridged branched chains running in the  $[100]$  direction, built by the repetition of  $[Mn(H_2O)\{Cr(ox)_3\}_2]^{4+}$  units (Figure 8; Table S7). Four 1-hydroxyethyl-4-(4'-dimethylamino- $\alpha$ -styryl)-pyridinium cations ensure the electroneutrality of the compound (Figure 9b). There are two crystallographically independent chromium(III) units with very similar bond lengths (Table S7). On the one hand, Cr(1) acts as bidentate ligand toward the manganese(II) ion through one oxalate

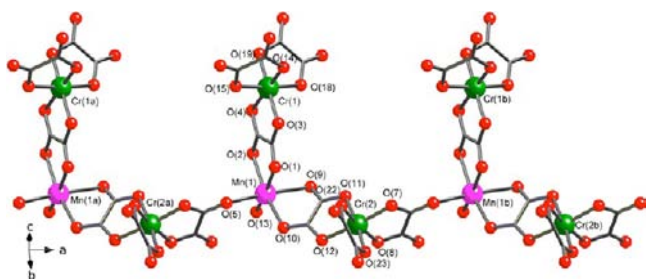


**Figure 8.** Compound 4: View of the  $[\text{Mn}(\text{H}_2\text{O})\{\text{Cr}(\text{ox})_3\}_2]^{4+}$  heterobimetallic unit showing the atom numbering [Symmetry codes: (a) =  $x - 1, y, z$ ; (b) =  $x + 1, y, z$ ].

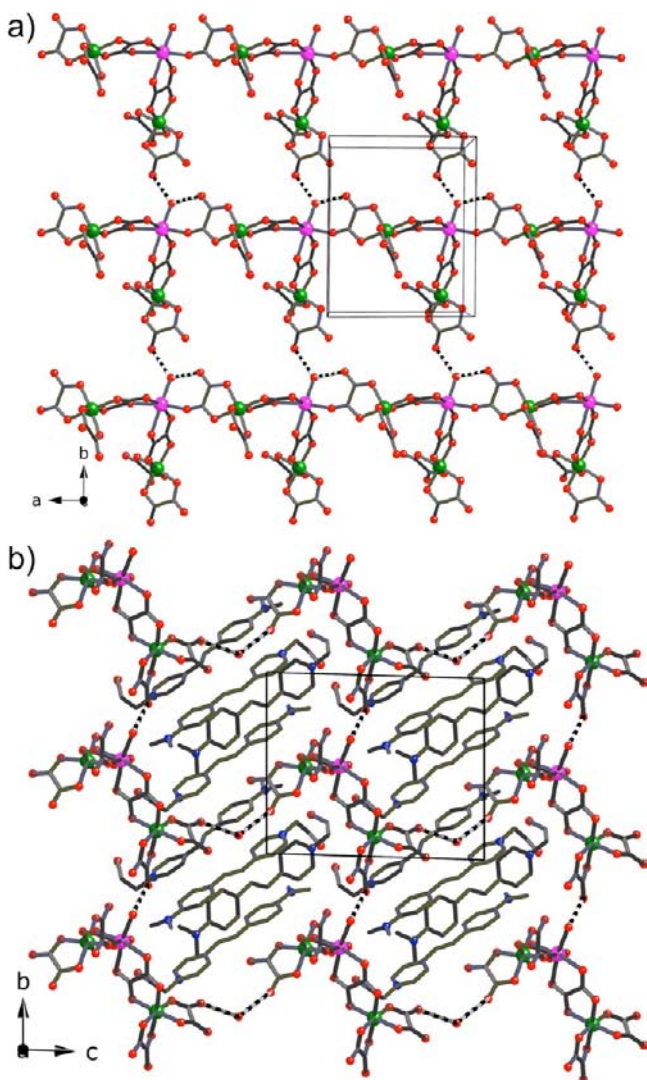


**Figure 9.** Compound 4: Crystal packing of the chains in the  $ab$  (a) and  $bc$  (b) planes. Same representation code as in Figure 1.

group, creating  $[\text{Mn}-\text{Cr}]$  pairs. The two other oxalate ligands do not coordinate. The  $[\text{Cr}(1)(\text{ox})_3]^{3-}$  moiety thus appears as a terminal metalloligand. On the other hand,  $\text{Cr}(2)$  is surrounded by: (i) one terminal oxalate, (ii) one bidentate oxalate toward  $[\text{Mn}(1)]$ , and (iii) one monodentate oxalate toward  $[\text{Mn}(1b)]$ , leading to the formation of chains along the  $a$  axis. In the chain, alternate the usual  $\text{Mn}(1)-(\mu\text{-ox-}1\kappa^1\text{O}^1, \text{O}^2:2\kappa^2\text{O}^3, \text{O}^4)-\text{Cr}(2)$  units with a bis(bidentate) coordination of the oxalate bridge  $[\text{Mn}(1)\cdots\text{Cr}(2) = 5.4960(8) \text{ \AA}]$  and

$\text{Cr}(2)-(\mu\text{-ox-}1\kappa^1\text{O}^1:2\kappa^2\text{O}^3, \text{O}^4)-\text{Mn}(1b)$  units where the monodentate coordination of the oxalate to the manganese lengthens the  $\text{Cr}-\text{Mn}$  distance  $[\text{Cr}(2)\cdots\text{Mn}(1b) = 6.1112(8) \text{ \AA}]$ . Accordingly, the  $\text{Mn}(\text{II})$  ions have a distorted octahedral environment  $[\text{MnO}_6]$  with five carbonyl oxygen atoms from three oxalate groups of the two  $[\text{Cr}(\text{ox})_3]^{3-}$  entities  $[\text{Mn}-\text{O} = 2.144(2)-2.312(2) \text{ \AA}]$  and one water molecule  $[\text{Mn}-\text{O}(\text{w}) = 2.133(2) \text{ \AA}]$  coordinated in a cis position with respect to the monodentate oxalate. Within one chain, both  $\text{Cr}(\text{III})$  and  $\text{Mn}(\text{II})$  ions adopt the  $\Lambda$  configuration leading to the formation of chiral helical chains. Due to the absence of improper symmetry element in the  $P1$  space group, the enantiomer is not present in the studied crystal. This indicates either a spontaneous resolution or a conglomerate. The lack of Cotton effect in the circular dichroism (CD) spectra acquired from a bulk sample of **4** (data not shown) confirms the second hypothesis.

In **4**, the neighboring chains are packed in the  $ab$  plane. They interact through a hydrogen bond between one of the oxygen atoms of the terminal oxalate and the water molecule coordinated to the manganese(II) ion  $\text{O}(13)-\text{H}(13\text{B})-\text{O}(16)$   $[\text{O}^-\text{O} = 2.7156(35) \text{ \AA}]$  leading to the formation of a square-like two-dimensional (2D) supramolecular motif combining coordination and hydrogen bonds (Figure 9a). The coordinated water molecule further interacts with the noncoordinating oxygen atom of the monodentate oxalate ligand  $\text{O}(13)-\text{H}(13\text{A})-\text{O}(6)$   $[\text{O}^-\text{O} = 2.7865(30) \text{ \AA}]$  (Figure 9a). In the  $ab$  plane, the branched chains are close. The distance between  $\text{Cr}(1)$  and the nearest manganese center is  $8.1869(11) \text{ \AA}$  whereas the intrachain  $\text{Cr}^-\text{Mn}$  distances are  $5.4960(8)-5.5694(9) \text{ \AA}$  (Figure 9a). Along the  $c$  axis, the chains are well separated from each other thanks to the presence of the stylbazonium cations (Figure 9b): the shortest interchain  $\text{Cr}^-\text{Cr}$ ,  $\text{Mn}^-\text{Mn}$ , and  $\text{Cr}^-\text{Mn}$  distance are much larger than those along the other directions, being  $10.4156(14)$ ,  $12.8130(12)$  and  $8.1869(11) \text{ \AA}$ , respectively. Along the  $c$  axis, the unique crystallization water molecule is engaged in two hydrogen bonds between two chains  $\text{O}(20)-\text{H}(26\text{A})-\text{O}(26)-\text{H}(26\text{B})-\text{O}(24)$   $[2.8882(35)-2.8309(35) \text{ \AA}]$ .

The organization of the hyperpolarizable stilbazonium cations in the  $P1$  non centrosymmetric spacegroup is complex (Figure 9b). The cations lie with their long axis approximately at  $45^\circ$  of the  $ac$  plane and their molecular plane at  $45^\circ$  of the oxalate layers. The cations are uniformly packed in groups of four with a resulting net dipolar moment aligned along the  $ac$  plane. However, despite the non-centrosymmetry of the space group, the head-to-tail arrangement of each pair of cations leads to a cancellation of the dipolar moment at the crystal level (Figure 9b).

**NLO Properties.** The ability of the non-centrosymmetric members of this new family of compounds with polar cations to display second harmonic generation (SHG) has been studied under IR light. Despite its noncentrosymmetric  $P1$  space group, compound **4** did not show any observable SHG signal in accordance with the arrangement of the hyperpolarizable cations (Figure 9b). On the contrary, compound **3** is NLO active with an efficiency up to 5–10 times that of urea at  $1.9 \mu\text{m}$ . The relatively important SHG response is related to the polarizable molecular structure of the 1-hydroxyethyl-4-dimethylaminopyridinium chromophores, and to their non-centrosymmetric packing arrangement. The extended  $J$ -type aggregates (Figure 7) bring about a large hyperpolarizability.<sup>26</sup>

**Magnetic Properties.** Manganese(II)–Chromium(III) Chains. The direct current (*dc*) magnetic properties of the chromium(III)–manganese(II) chains in the form of  $\chi_M T$  versus  $T$  plot ( $\chi_M$  is the magnetic susceptibility per [MnCr] pair for **1**, **2a**, and **3** and per [MnCr<sub>2</sub>] unit for **4**, and  $T$  is the temperature) are shown in Figures 10 (**1**, **2a**, and **3**) and 11

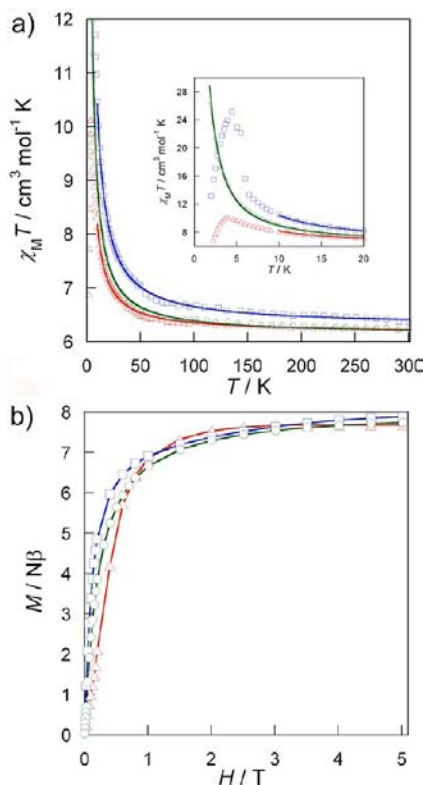


**Figure 10.** (a) Temperature dependence of  $\chi_M T$  for **1** ( $\Delta$ , red), **2a** ( $\square$ , blue), and **3** ( $\circ$ , green). The inset shows the low temperature region and the maxima for **1** and **3**. The solid lines correspond to the fit based on Monte Carlo simulations (see text). (b) Field dependence of the magnetization  $M$  for a MnCr pair of **1** ( $\Delta$ ), **2a** ( $\square$ ), and **3** ( $\circ$ ) at  $T = 2.0$  K. The solid lines are guides for the eye.

(**4**). The values of  $\chi_M T$  at room temperature vary in the narrow range of  $6.24$ – $6.37$   $\text{cm}^3 \text{mol}^{-1} \text{K}$  for **1**, **2a**, and **3**. They closely correspond to the value calculated for the sum of a Cr<sup>III</sup> ion ( $S_{\text{Cr}} = 3/2$ ;  $g_{\text{Cr}} = 2.0$ ) and a high-spin (HS) Mn<sup>II</sup> ion ( $S_{\text{Mn}} = 5/2$ ;  $g_{\text{Mn}} = 2.0$ ) magnetically isolated. For compound **4**, the value of  $\chi_M T$  at room temperature of  $8.18$   $\text{cm}^3 \text{mol}^{-1} \text{K}$  is in line with the [MnCr<sub>2</sub>] stoichiometry.

Upon cooling,  $\chi_M T$  for **1**, **2a**, and **3** increases slowly in the  $300$ – $30$  K temperature range, then it increases much rapidly to reach maxima at  $3.7$  and  $4.3$  K with  $\chi_M T$  values of  $10.1$  (**1**) and  $25.3$  (**2a**)  $\text{cm}^3 \text{mol}^{-1} \text{K}$ , respectively. For **3**,  $\chi_M T$  reaches  $26.3$   $\text{cm}^3 \text{mol}^{-1} \text{K}$  at  $2.0$  K without maximum.  $\chi_M$  maxima are observed at  $2.5$  K for **1** and  $2.6$  K for **2a**. For **4**,  $\chi_M T$  increases and presents a maximum at  $7.5$  K ( $\chi_M T = 9.47$   $\text{cm}^3 \text{mol}^{-1} \text{K}$ ) and then decreases. For the four compounds, the increase of  $\chi_M T$  when decreasing the temperature is the signature of an intrachain ferromagnetic coupling. The decrease observed at low temperature for **1** and **2a** reveals weak interchain antiferromagnetic interactions ( $J'$ ) in the two compounds the intensity of which is related to the temperature where the value of the maximum of  $\chi_M T$  occurs  $|J'(\mathbf{2a})| > |J'(\mathbf{1})| > |J'(\mathbf{3})|$ .

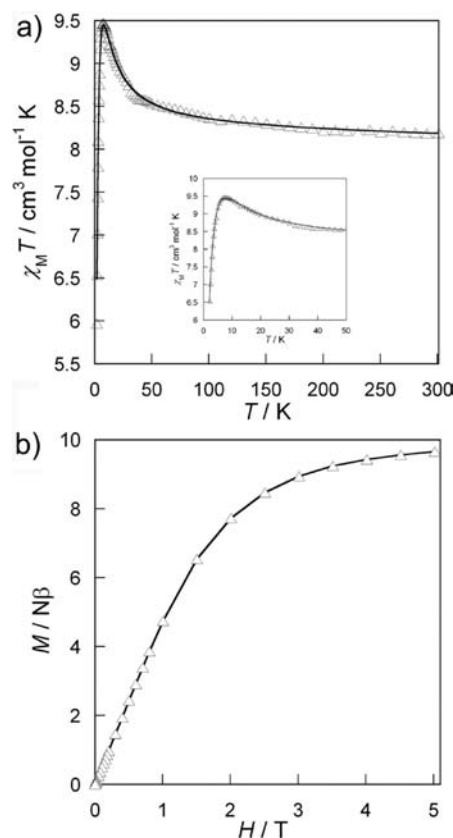


**Figure 11.** (a) Temperature dependence of  $\chi_M T$  for **4** ( $\Delta$ ). The inset shows the  $\chi_M T$  maximum. The solid line corresponds to the best fit (see text). (b) Field dependence of  $M$  of **4** ( $\Delta$ ) at  $2.0$  K. The solid line is a guide for the eye.

The magnetization  $M$  vs the applied magnetic field  $H$  plots for **1**, **2a**, and **3** at  $2.0$  K are shown in Figure 10b. The saturation values ( $7.56$ – $7.88$   $N\beta$  at  $5.0$  T) are reached rapidly and they are consistent with a  $S = 4$  ferromagnetic spin ground state of the [MnCr] pairs. For **4**, the  $M_S$  value ( $9.66$   $N\beta$  at  $5.0$  T) fits well with a ferromagnetic alignment of the spins in the [MnCr<sub>2</sub>] unit. Nevertheless, the higher fields necessary to reach the saturation reveal antiferromagnetic interactions between the [MnCr<sub>2</sub>] fragments.

The magnetic susceptibility of **1**, **2a**, and **3** was modeled through Quantum Monte Carlo (QMC) calculations by using a bimetallic 1D model (see Computational Details in Experimental Section). The QMC polynomial expression of  $\chi_M T$  (eq 1) was used for a least-squares fitting of the experimental data in the temperature ranges  $10$ – $300$  K (**1** and **2a**) and  $1.8$ – $300$  K (**3**) (Figure 10a). The values of the best-fit parameters are  $J = +0.55$  (**1**),  $+1.02$   $\text{cm}^{-1}$  (**2a**) and  $+0.75$   $\text{cm}^{-1}$  (**3**),  $g_{\text{Cr}} = g_{\text{Mn}} = 1.99$  (**1**),  $2.02$  (**2a**), and  $1.98$  (**3**) with  $F = 1.6 \times 10^{-5}$  (**1**),  $1.4 \times 10^{-5}$  (**2a**), and  $3.3 \times 10^{-5}$  (**3**).

For compound **4**, we first considered the magnetic susceptibility of independent trinuclear [MnCr<sub>2</sub>] units by full-matrix diagonalization<sup>27</sup> of the isotropic spin Hamiltonian (eq 2) within the mean field approximation with  $S_{\text{Mn}} = 5/2$  and  $S_{\text{Cr1}} = S_{\text{Cr2}} = 3/2$ :

$$\hat{H} = -J[\hat{S}_{\text{Mn}} \cdot \hat{S}_{\text{Cr1}} + \hat{S}_{\text{Mn}} \cdot \hat{S}_{\text{Cr2}}] + g_{\text{Mn}} \hat{S}_{\text{Mn}} H + g_{\text{Cr}} [\hat{S}_{\text{Cr1}} + \hat{S}_{\text{Cr2}}] H \quad (2)$$

where  $J$  is the intramolecular exchange interaction through the bis(bidentate) oxalate bridges within the trinuclear units.

The interactions between the trinuclear units were then taken into account by introducing a Curie–Weiss temperature  $\theta$ . The fitted curve closely follows the experimental data in the temperature range 2–300 K (Figure 11a). The least-squares fit of the experimental data gives  $g = g_{\text{Cr}} = g_{\text{Mn}} = 2.00$ ,  $J = +2.07 \text{ cm}^{-1}$ , and  $\theta = -2.35 \text{ cm}^{-1}$ .

The structure reveals that the interchain contacts in **4** should be weak as in **1–3**. Accordingly, we suggest that the negative Curie–Weiss parameter determined for **4** is essentially due to the antiferromagnetic intrachain exchange interaction between the  $[\text{MnCr}_2]$  units.

**Cobalt(II)–Chromium(III) Chains.** The  $\chi_{\text{M}}T$  versus  $T$  plot for **2b** ( $\chi_{\text{M}}$  being the magnetic susceptibility per  $[\text{CoCr}]$  pair) is shown in Figure 12a. The value of  $\chi_{\text{M}}T$  at room temperature is

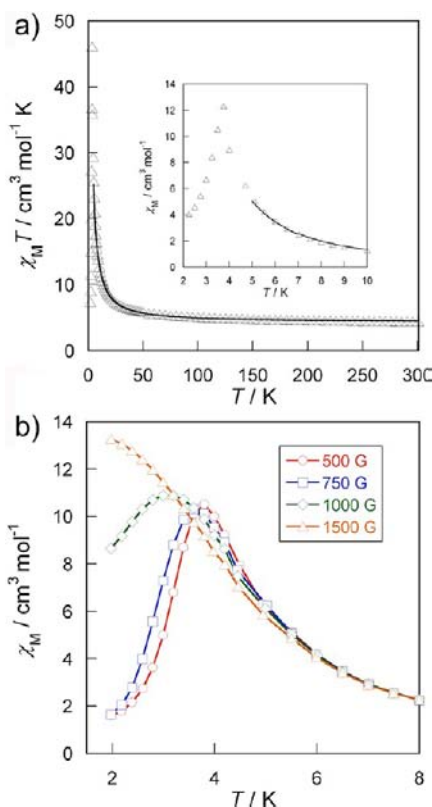


**Figure 12.** (a) Temperature dependence of  $\chi_{\text{M}}T$  for **2b** ( $\Delta$ ). The inset emphasizes the maximum of  $\chi_{\text{M}}$  at low temperature. (b)  $\chi_{\text{M}}$  versus  $T$  plot of **2b** as a function of the applied magnetic field at low temperature.

$4.40 \text{ cm}^3 \text{ mol}^{-1} \text{ K}$ . It corresponds to the sum of a magnetically isolated  $\text{Cr}^{\text{III}}$  ion ( $S_{\text{Cr}} = 3/2$ ;  $g_{\text{Cr}} = 2.0$ ) and a HS octahedral  $\text{Co}^{\text{II}}$  ion ( $S_{\text{Co}} = 3/2$ ) with an important orbital contribution ( $g_{\text{Co}} = 2.5$ ).<sup>28</sup> Upon cooling,  $\chi_{\text{M}}T$  increases suggesting a ferromagnetic intrachain interaction (Figure 12a), and reaches a maximum at 3.7 K ( $40.0 \text{ cm}^3 \text{ mol}^{-1} \text{ K}$ ) before decreasing abruptly.

The susceptibility of **2b** becomes field dependent for  $T < 6 \text{ K}$  (Figure 12b). A maximum is observed for applied magnetic inductions lower than 0.1 T (Figure 12b) and disappears at higher values. This suggests a field-induced transition from an antiferromagnetic to a ferromagnetic ground state. The sigmoidal shape of the isothermal  $M$  vs  $H$  plots (Figure 13a) with a crossing point at ca. 0.1 T, agrees with a metamagnetic-

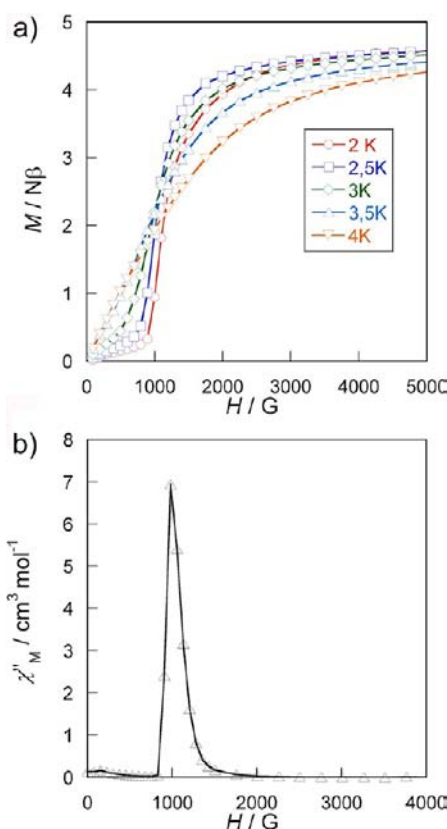


**Figure 13.** (a) Isotherms ( $2 \text{ K} \leq T \leq 4 \text{ K}$ ) of the magnetization versus  $H$  plot for **2b**. (b)  $\chi''_{\text{M}}$  versus  $H$  plot of **2b** at 2 K.

like behavior. The transition from an antiferro- to a ferromagnetic ordering is confirmed by the sharp peak at 0.1 T of the out-of-phase  $ac$  molar magnetic susceptibility  $\chi''_{\text{M}}$  vs  $H$ .

The value of the magnetization at saturation per  $[\text{CoCr}]$  pair, at 2.0 K of  $4.86 N\beta$  at 5.0 T is consistent with the calculated saturation magnetization corresponding to a parallel alignment of the effective spin of  $\text{Co}^{\text{II}}$  ( $S_{\text{Co}}^{\text{eff}} = 1/2$ ) and the spin of  $\text{Cr}^{\text{III}}$  ( $S_{\text{Cr}} = 3/2$ ) [ $M_{\text{s}} = (g_{\text{Co}}^{\text{eff}} S_{\text{Co}}^{\text{eff}} + g_{\text{Cr}} S_{\text{Cr}}) N_{\text{A}} \beta = 5.15 N\beta$  with  $g_{\text{Co}}^{\text{eff}} = 4.3$  and  $g_{\text{Cr}} = 2.0$ ].

The magnetic susceptibility data of **2b** above 6 K was analyzed through Quantum Monte Carlo (QMC) calculations as for the  $[\text{MnCr}]$  chains (see Computational Details). The least-squares fitting of the experimental data in the temperature range 10–300 K reproduces well the experimental data (Figure 12a). The best-fit parameters are  $J = +3.83 \text{ cm}^{-1}$ ,  $g_{\text{Cr}} = 2.00$  (fixed),  $g_{\text{Co}} = 2.31$ , with  $F = 2.2 \times 10^{-4}$ .

The nature of the exchange interaction found in the studied one-dimensional compounds is the same as in the previously described discrete oxalate-bridged polynuclear complexes.<sup>13–18</sup> For compounds **2** and **4**, the magnitude of the exchange is comparable to the previously observed values whereas, for compounds **1** and **3**, it drops below  $1 \text{ cm}^{-1}$ , at significantly lower values than generally observed in  $\text{Mn}(\text{II})$ – $\text{Cr}(\text{III})$  oxalate-bridged systems.

## DISCUSSION

In the present work, we take advantage of the versatility of molecular chemistry to combine oxalate-bridged bimetallic architectures with polar cations within the same material. The former partner is chosen for its magnetic properties whereas the latter may introduce properties related to its polar character,

e.g. aminopyridinium derivatives are indeed known for their ferroelectric properties,<sup>5f,29</sup> whereas 4-(4'-dimethylamino- $\alpha$ -styryl)-pyridinium exhibits nonlinear optical properties both in solution and in the solid state.<sup>9,10</sup> From a synthetic point of view, the use of  $(\text{NH}_4)_3[\text{Cr}(\text{ox})_3]\cdot 3\text{H}_2\text{O}$  is a valuable way for introducing tris(oxalate)chromate(III) in a mixed water/organic solvent to solubilize organic partners. However, we recently demonstrated that the ammonium ion may compete with the organic cation in templating the oxalate-bridged architecture.<sup>5e</sup> Thus, we performed a metathesis from  $(\text{NH}_4)_3[\text{Cr}(\text{ox})_3]\cdot 3\text{H}_2\text{O}$  toward  $(\text{C}_x)_3[\text{Cr}(\text{ox})_3]\cdot n\text{H}_2\text{O}$  before introducing the metal(II) salt in solution. We obtained various topologies in a series of one-dimensional compounds, a dimensionality scarcely observed in bimetallic oxalate-bridged systems.<sup>18</sup> Recent examples have reported the insertion of 1-methyl-4-(4'-dimethylamino- $\alpha$ -styryl)-pyridinium as counterion in 1D compounds whereas this cation has been previously introduced in 2D oxalate-bridged bimetallic networks.<sup>9,10</sup> We try, in the following paragraphs, to identify and to understand the parameters that control the dimensionality and the topology of the compounds to allow their rational synthesis.

The first important point is to use a robust, magnetic building block. This is the main reason for the choice of the  $[\text{Cr}(\text{ox})_3]^{3-}$  moiety. It is stable due to the chelating property of oxalate and inert because of the  $d^3$  electronic structure of the chromium(III). In all the described compounds, the  $[\text{Cr}(\text{ox})_3]^{3-}$  precursor is fully preserved as a  $D_3$  symmetry synthon. The  $[\text{Cr}(\text{ox})_3]^{3-}$  anionic complex is a good Lewis base able to strongly bind metallic Lewis acids in three different spatial directions, a feature well suited for the complex-as-ligand strategy, which is an important milestone in the rational design of complex metal–organic architectures.

The second important point is the choice of the second metallic precursor to open access to various coordination environments. A divalent cation allows obtaining an anionic  $[\text{M}(\text{II})\text{Cr}(\text{III})(\text{ox})_3]^-$  repeating unit<sup>17d</sup> preparing the later insertion of the third partner, i.e. the organic cation. The heteroleptic character of the M(II) center, with a potentially variable coordination environment is as important as the homoleptic character of the Cr(III). The choice of Mn(II) and, to a lesser extent, Co(II) guarantees the flexibility of the coordination sphere. The Mn(II) radius and the Mn(II)-ligand distances are larger than those observed with the other divalent transition metal ions because of the antibonding role of the  $e_g$  electrons in an octahedral surrounding. It makes it possible to accommodate more ligands and to reach coordination numbers higher than six. Indeed, important variations in the environment of the metal(II) ion can be observed in the series of compounds herein described. In **2** and **4**, the metal(II) is hexacoordinated, while in **1** and **3**, the manganese(II) ion is heptacoordinated. Octacoordinated Mn(II) centers have also been observed in oxalate-bridged compounds.<sup>5e,14a</sup> Obviously, this Mn(II) coordination versatility can open routes to other dimensionalities when varying the synthetic conditions. For example, a change from hexa- to hepta-coordination influences the organization of 2D networks but does not prevent their formation<sup>5f,11f</sup> whereas a 3D network implying octacoordinated manganese(II) has been described.<sup>5e</sup>

The third important point is the oxalate ligand itself. The versatility of the coordination mode of this ligand is well-known and well exemplified in this series of compounds: it remains terminal as observed in **1–4**; it binds to the metal(II) ion in a monodentate mode as found in **4** for one of the oxalate or,

most often, in a bidentate manner leading to the bis(bidentate) bridging situation in **1–4**. The monodentate binding mode of the metal(II) ion is scarce. It has been previously observed in a 2D network.<sup>11f</sup> The coexistence around the Cr(III) of one nonbonding mode and two bis(bidentate) modes of the oxalate is crucial to get 1D compounds (**1–4**).

A fourth important point is the choice of the synthetic conditions to offer the suitable ligands to complete the coordination sphere of the metal(II) ion: solvent (water, alcohol), ancillary anions (chloride), organic cations. The Lewis base character of these potential ligands controls the coordination. The nature of each coordinated ligand opens the way to different intermolecular interactions and hence different topologies. Three different coordinated ligands are present in this study. First, a chloride ion is coordinated to the metal(II) ion in one type of the chains encountered in **2**. It has only a blocking role. It is neither bridging nor implied in H-bonding. Second, water molecules are coordinating in **1**, **2**, and **4**. They occupy a M(II) coordination position but they are also implied in hydrogen bonds with neighboring molecules. Third, in **3**, the amino-pyridinium  $\text{C}_3^+$  acts as a ligand through its alcoholic functional group. This last case appears surprising. It has never been observed before and it contrasts with the one observed for the polymorph of formula  $(\text{C}_3)[\text{MnCr}(\text{ox})_3(\text{CH}_3\text{CH}_2\text{OH})]$  which consists of 2D anionic  $[\text{MnCr}(\text{ox})_3(\text{C}_2\text{H}_5\text{OH})]^-$  layers, interleaved by stacks of the polar cation  $\text{C}_3^+$  whereas the neutral ethanol molecule is coordinated to manganese(II).<sup>5f</sup> The ratio EtOH– $\text{H}_2\text{O}$  in the reaction mixture is the key point that accounts for the shift between the two structures. A competition exists between the two weak Lewis bases alcohols [ethanol and 4-*N,N*-dimethylamino-1-hydroxyethylpyridinium] to coordinate the Lewis acidic manganese(II) ions. When using a slow diffusion technique (ethanol diffusion in aqueous solution), the ethanol concentration is not high enough to prevent 4-*N,N*-dimethylamino-1-hydroxyethyl-pyridinium cation from coordinating and the neutral 1D compound **3** crystallizes in the polar aqueous solvent. The electrostatic interaction between the anionic network and the organic cation helps the coordination process. Instead, when using a 9:1 EtOH– $\text{H}_2\text{O}$  ratio, the ethanol molecules coordinate, the  $\text{C}_3^+$  cation and the anionic network remain in solution, and the system crystallizes after some days in a completely different thermodynamic potential well and 2D structure.<sup>5f</sup>

Another important feature in this series of compounds is that the  $[\text{Cr}(\text{ox})_3]^{3-}$  moiety essentially acts as bis(bidentate) metalloligand. This behavior is scarce<sup>10,17,18</sup> and contrasts with its tris(bidentate) metalloligand ability in the formation of 2D and 3D metal–organic frameworks (MOFs).<sup>11,12</sup> In **4**,  $[\text{Cr}(\text{ox})_3]^{3-}$  even acts as a single connector leading to an original branched topology. This behavior is similar to what has been observed in the formation of dinuclear and trinuclear complexes.<sup>17</sup> In all the cases where the coordination connectivity of the chromium(III) complex is restricted, the terminal oxalates are engaged in hydrogen bonds that imply coordination or coordinated water molecules. This competition between hydrogen and coordination bonds appears as an essential point to prevent the formation of coordination extended networks. It should be noted that, in most cases, the coordination and hydrogen bonds combine to form complex supramolecular motifs that are reminiscent of those observed in extended coordination networks as shown in Figures 2 and 6. In **1**, the tetramethylammonium cation sits

strictly in the 2D supramolecular anionic network, whereas in purely coordinative oxalate-bridged 2D networks, only one alkyl of tetraalkylammonium enters into the cell.<sup>5b</sup> Because of this location, despite a smaller overall size, the tetramethylammonium cation prevents the ring closure toward the usual purely coordinative honeycomb motifs and favors the observed supramolecular organization with elongated honeycomb cells. The situation is comparable in **3**: the coordinated cation  $C_3^+$  of two adjacent chains are  $\pi$ -stacked at the center of a supramolecular honeycomb motif (Figure 6a). The ring closure is then ensured by H-bonds between the terminal oxalate of one chain and the alcoholic function of  $C_3^+$  on the one hand [ $O(12)-O(13) = 2.7069(32)$  Å] and between the second terminal oxygen atom of the oxalate and a coordinated water molecule on the other hand. This last case indicates that when functional groups are chosen to favor the introduction of new physical properties, the prediction of the structure is more difficult. These actors deeply modify the possible intermolecular interactions and hence make new topologies possible. This is particularly true with polar functional groups able to establish hydrogen and coordination bonds as those we are currently studying for introducing SHG and ferroelectric properties. In turn, it appears that such cations tend to favor the formation of low dimensional systems.<sup>10,17,18</sup>

Even if we understand better how to reach the various topologies, we should recognize that, at the present stage, important features are still out of a priori control: (i) the subtle weak supramolecular interactions tuning the Madelung energy which determines the exact organization of the molecular ions in the ionic crystal; (ii) the non centrosymmetrical character of the space groups of **3** ( $C2cb$ ) and **4** ( $P1$ ); the appearance of a unique enantiomer from a initial racemic bath is still an intriguing problem—and ever fascinating for living organisms—and one of our present lines of research.<sup>5b,e,f,17a</sup>

Concerning the nonlinear optical (NLO) properties, despite the presence of hyperpolarizable cations in **2a**, **2b**, **3**, and **4**, only compound **3** was found to be NLO active. Complexes **2a** and **2b** belong to the centrosymmetric  $P2_1/c$  space group, which accounts for their NLO inactivity. Compound **4**, despite its crystallization in a noncentrosymmetric space group ( $P1$ ), presents an average centrosymmetrical organization of the polar cations (see structural section) preventing the observation of these properties.

The magnetic properties of the one-dimensional compounds **1–4** are examined in the light of the crystal structure. They are influenced by both the 1D structures and by the interchain interactions. In all the compounds **1–4**, the  $[Cr(ox)_3]^{3-}$  moiety provides three unpaired electrons in  $t_{2g}$  orbitals considering the  $CrO_6$  polyhedron as an octahedron. On the other hand, Mn(II) provides five unpaired electrons (three  $t_{2g}$ , two  $e_g$  when the manganese(II) surrounding is octahedral). When the bridging oxalate is bis(bidentate) (i) the  $Cr(t_{2g})$  and  $Mn(t_{2g})$  orbitals weakly overlap and the corresponding antiferromagnetic interactions are weak; (ii) the  $Cr(t_{2g})$  and  $Mn(e_g)$  orbitals are orthogonal and provide a significant ferromagnetic contribution specially through the  $Mn d_{x^2-y^2}$  orbital. The overall interaction is therefore weak and ferromagnetic. DFT calculations confirm this analysis and underline that we are located close to the crossing point between the ferromagnetic and antiferromagnetic regime depending on the details of the structure of the bridge.<sup>14d,17a</sup> In compounds **1**, **2a**, **3**, and **4**, we retrieve a weak ferromagnetic Mn(II)–Cr(III) exchange interaction mediated by the bis(bidentate) oxalate ligand. In compound **4**, it is also

found within the  $[MnCr_2]$  units. The Mn(II)–Cr(III) ferromagnetic interaction is experimentally robust in the bis(bidentate) coordination mode though we observe a weakening of the interaction when the coordination sphere of the manganese(II) departs from the octahedron. This variation is somehow reflected by the drop of  $T_C$  in 2D oxalate-bridged compounds where such a coordination of the manganese(II) is observed.<sup>5f</sup> Thanks to the quantitative treatment of the magnetic susceptibility in low dimensional systems, it is possible to quantify this influence of the change of coordination environment of the manganese(II) ion.<sup>14d,17a</sup>

The influence of the bridging mode of the oxalate is more dramatic than the one of the manganese coordination sphere, and appears as the key parameter governing the nature of the coupling: the exchange interaction sweeps from ferromagnetic for the bis(bidentate) bridging mode to antiferromagnetic for the bidentate–monodentate bridging mode observed between the  $[MnCr_2]$  trinuclear units of **4**, as once previously observed.<sup>11f</sup> This rocking from a ferromagnetic to antiferromagnetic exchange interaction is related to the switch from strict orthogonality in the  $Mn(e_g)-Cr(t_{2g})$  exchange pathways to increased overlap upon oxalate bridge dissymmetrization.

The interchain interactions (hydrogen bond contacts,  $\pi-\pi$  interactions, etc.) are also reflected in the magnetic properties. **1** and **2a** show maxima in the  $\chi_M T$  vs  $T$  plots because of the antiferromagnetic coupling coming from an efficient interaction between neighboring chains. On the contrary, in **3**, despite the fact that the neighboring chains are close to each other no maximum in the  $\chi_M T$  vs  $T$  plot is observed, indicating that this structural feature is not reflected by the magnetic properties in the observed temperature range. More dramatically, these antiferromagnetic interactions, associated with the larger magnetic anisotropy of the  $Co^{II}$  ions, are responsible for the metamagnetic behavior with a  $H_C$  value of 1000 G observed in compound **2b**.

## CONCLUSION

In this manuscript, we have described the synthesis and the structural, NLO, and magnetic properties of five bimetallic oxalate-bridged chains. By using  $(C_x)_3[Cr^{III}(ox)_3]$  salts as precursors, the synthetic strategy combined the well-known “complex-as-ligand” strategy with a preliminary metathesis to restrict the possibilities of self-assembly and increase the predictability of the system evolution. The use of the  $[Cr^{III}(ox)_3]^{3-}$  unit yielded in all cases one-dimensional compounds where at least one of the oxalate ligands remained nonbridging in contrast with the well-known 2D or 3D bimetallic metal–organic frameworks.<sup>30</sup> Up to date, this bis(bidentate) coordination mode was only seen in a few one-dimensional and discrete trinuclear compounds.<sup>10,17,18</sup> We speculate that the polar cations play an important role in the assembly process, whether by means of insolubility of the formed species, steric hindrance, or intermolecular interactions.

The inclusion of hyperpolarizable chromophores in these ferromagnetic systems yielded SHG active magnets when a noncentrosymmetric assembly of the chromophores was reached as in the case of **3**.

The variety of architectures observed for these five compounds is reflected in their magnetic behavior. **1** and **2a** show maxima in the  $\chi_M$  vs  $T$  plots related to significant antiferromagnetic interchain interactions whereas the isolation of the chains in **3** prevents the presence of a maximum of  $\chi_M$  in the explored temperature range. More dramatically, the

metamagnetic behavior of compound **2b** is due to the combination of weak interchain antiferromagnetic interactions together with the magnetic anisotropy of Co(II) ions. The variations of the coordination environment of the metal(II) ions as well as the two bridging modes of the oxalate observed along this series of compounds lead to the conclusion that the key parameter of the M(II)–Cr(III) exchange interaction is the bridging mode of the oxalate rather than the coordination number or the nature of the oxalate coligands of the metal(II) ion: a bis(bidentate) bridging mode favors a ferromagnetic exchange between the neighboring metal ions<sup>14d,17a</sup> whereas a bidentate–monodentate bridging mode leads to an antiferromagnetic interaction.

## ■ ASSOCIATED CONTENT

### Supporting Information

Experimental preparation and synthesis of C<sub>4</sub>I (Scheme S1), analytical and spectroscopic characterization of all the compounds reported (Tables S1–S2), selected bonds and angles for compounds 1–4 (Tables S3–S7), polynomial coefficients for eq 1 (Tables S8–S9). This material is available free of charge via the Internet at <http://pubs.acs.org>.

## ■ AUTHOR INFORMATION

### Corresponding Author

\*E-mail: [michel.verdaguer@upmc.fr](mailto:michel.verdaguer@upmc.fr) (M.V.), [cyrille.train@lncmi.cnrs.fr](mailto:cyrille.train@lncmi.cnrs.fr) (C.T.).

### Notes

The authors declare no competing financial interest.

## ■ ACKNOWLEDGMENTS

This work was supported by the Centre National de la Recherche Scientifique (CNRS, France), the Ministère de l'Enseignement Supérieur et de la Recherche (MESR, France), the Agence Nationale de la Recherche (ANR, France ; project ANR-08-JCJC-0113-01), the University of Valencia (Spain) (Project UV-INV-AE11-38904), and the Generalitat Valenciana (Spain) (Project GV/2012/051). PRES UniverSud is acknowledged for its support for SHG equipment. E.P. acknowledges the MICIIN (Spain) for his postdoctoral grant.

## ■ REFERENCES

- (1) (a) Werner, A. *Ber.* **1912**, *45*, 3061. (b) Werner, A.; Poupardin, J. *Ber.* **1914**, *47*, 1954.
- (2) (a) Kahn, O. *Molecular Magnetism*; VCH, New York, 1993. (b) *Magneto-Structural Correlation in Exchange Coupled Systems*; Eds. Willet, R. D., Gatteschi, D., Kahn, O.; NATO ATI Series C140; Reidel: Dordrecht, 1985. (c) Caneschi, A.; Gatteschi, D.; Pardi L.; Sessoli, R. In *Perspectives in Coordination Chemistry*; Eds. Williams, A. F., Floriani, C., Merbach, A. E.; Verlag: Basel, 1992; p 109. (d) Braunstein, P. In *Perspectives in Coordination Chemistry*; Eds. Williams, A. F., Floriani, C., Merbach, A.; Verlag: Basel, 1992; p 67. (e) *Molecular Magnetic Materials*; Eds. Gatteschi, D., Kahn, O., Miller, J.; NATO ASI Series E198; Kluwer: Dordrecht, 1991. (f) *Molecular Magnetism: From Molecular Assemblies to the Devices*; Eds. Coronado, E., Delhaès, P., Gatteschi, D., Miller, J.; NATO ASI Series E321; Kluwer: Dordrecht, 1996. (g) *Supramolecular Engineering of Synthetic Metallic Materials*; Eds. Veciana, J., Rovira, C., Amabilino, D. B.; NATO ASI Series C518; Kluwer: Dordrecht, 1999.
- (3) (a) Scott, K. L.; Wieghardt, K.; Sykes, A. G. *Inorg. Chem.* **1973**, *12*, 655. (b) Le Floch, F.; Sala Pala, J.; Guerschais, J. *Bull. Soc. Chim. Fr.* **1975**, 1–2, 120. (c) Berezovsky, F.; Hajem, A. A.; Triki, S.; Sala Pala, J.; Molinie, P. *Inorg. Chim. Acta* **1998**, *284*, 8.
- (4) (a) Julve, M.; Verdaguer, M.; Charlot, M. F.; Kahn, O. *Inorg. Chim. Acta* **1984**, *82*, 5. (b) Julve, M.; Verdaguer, M.; Gleizes, A.; Philoche-Levisalles, M.; Kahn, O. *Inorg. Chem.* **1984**, *23*, 3808.
- (5) (a) Coronado, E.; Galán-Mascarós, J. R.; Gomez-Garcia, C. J.; Laukhin, V. *Nature* **2000**, *408*, 447. (b) Train, C.; Gheorghe, R.; Krstic, V.; Chamoreau, L. M.; Ovanesyan, N. S.; Rikken, L. J. A.; Gruselle, M.; Verdaguer, M. *Nat. Mater.* **2008**, *9*, 729. (c) Train, C.; Nuida, T.; Gheorghe, R.; Gruselle, M.; Ohkoshi, S. I. *J. Am. Chem. Soc.* **2009**, *131*, 16838. (d) Okawa, H.; Shigematsu, A.; Sadakiyo, M.; Miyagawa, T.; Yoneda, K.; Ohba, M.; Kitagawa, H. *J. Am. Chem. Soc.* **2009**, *131*, 13516. (e) Pardo, E.; Train, C.; Gontard, G.; Boubekeur, K.; Fabelo, O.; Liu, H.; Dkhil, B.; Lloret, F.; Nakagawa, K.; Tokoro, H.; Ohkoshi, S. I.; Verdaguer, M. *J. Am. Chem. Soc.* **2011**, *133*, 15328. (f) Pardo, E.; Train, C.; Liu, H.; Chamoreau, L.-M.; Dkhil, B.; Boubekeur, K.; Lloret, F.; Nakatani, K.; Tokoro, H.; Ohkoshi, S. I.; Verdaguer, M. *Angew. Chem., Int. Ed.* **2012**, *51*, 8356. (g) Clemente-León, M.; Coronado, E.; Martí-Gastaldo, C.; Romero, F. M. *Chem. Soc. Rev.* **2011**, *40*, 473. (h) Train, C.; Gruselle, M.; Verdaguer, M. *Chem. Soc. Rev.* **2011**, *40*, 3297.
- (6) Zyss, J. *Molecular Nonlinear Optics*; Academic Press: New York, 1994.
- (7) Marder, S. R. In *Inorganic Materials*, 2nd ed; O'Hare, D., Bruce, D. W., Eds.; John Wiley: Chichester, 1996.
- (8) Dalton, L. R.; Steier, W. H.; Robinson, B. H.; Zhang, C.; Ren, A.; Garner, S.; Chen, A. T.; Londergan, T.; Irwin, L.; Carlson, B.; Fifield, L.; Phelan, G.; Kincaid, C.; Amend, J.; Jen, A. *J. Mater. Chem.* **1999**, *9*, 1905.
- (9) (a) Benard, S.; Yu, P.; Audiere, J. P.; Riviere, E.; Clement, R.; Guilhem, J.; Tchertanov, L.; Nakatani, K. *J. Am. Chem. Soc.* **2000**, *122*, 9444. (b) Evans, J. S. O.; Benard, S.; Pei, Y.; Clement, R. *Chem. Mater.* **2001**, *13*, 3813. (c) Gruselle, M.; Malézieux, B.; Bénard, S.; Train, C.; Guyard-Duhayon, C.; Gredin, P.; Tonsuaadu, K.; Clément, R. *Tetrahedron Assym.* **2004**, *15*, 3103.
- (10) (a) Cariati, E.; Macchi, R.; Roberto, D.; Ugo, R.; Galli, S.; Casati, N.; Macchi, P.; Sironi, A.; Bogani, L.; Caneschi, A.; Gatteschi, D. *J. Am. Chem. Soc.* **2007**, *129*, 9410. (b) Cariati, E.; Ugo, R.; Santoro, G.; Tordin, E.; Sorace, L.; Caneschi, A.; Sironi, A.; Macchi, P.; Casati, N. *Inorg. Chem.* **2010**, *49*, 10894.
- (11) (a) Tamaki, H.; Zhong, Z. J.; Matsumoto, N.; Kida, S.; Koikawa, M.; Achiwa, N.; Hashimoto, Y.; Okawa, H. *J. Am. Chem. Soc.* **1992**, *114*, 6974. (b) Decurtins, S.; Schmalle, H. W.; Oswald, H. R.; Linden, A.; Enslin, J.; Guetlich, P.; Hauser, A. *Inorg. Chim. Acta* **1994**, *216*, 65. (c) Gruselle, M.; Andrés, R.; Malézieux, B.; Brissard, M.; Train, C.; Verdaguer, M. *Chirality* **2001**, *13*, 712. (d) Clemente-Leon, M.; Coronado, E.; Dias, J. C.; Soriano-Portillo, A.; Willett, R. D. *Inorg. Chem.* **2008**, *47*, 6458. (e) Duan, Z.; Zhang, Y.; Zhang, B.; Pratt, F. L. *Inorg. Chem.* **2009**, *48*, 2140. (f) Coronado, E.; Galán-Mascarós, J. R.; Martí-Gastaldo, C.; Murcia-Martínez, A. *Dalton Trans.* **2006**, 3294.
- (12) (a) Decurtins, S.; Schmalle, H. W.; Schneuwly, P.; Enslin, J.; Gütlich, P. *J. Am. Chem. Soc.* **1994**, *116*, 9521. (b) Coronado, E.; Galán-Mascarós, J. R.; Gómez-García, C. J.; Martínez-Agudo, J. M. *Inorg. Chem.* **2001**, *40*, 113. (c) Ballester, G.; Coronado, E.; Giménez-Saiz, C.; Romero, F. M. *Angew. Chem., Int. Ed.* **2001**, *40*, 792.
- (13) (a) Triki, S.; Berezovsky, F.; Pala, J. S.; Coronado, E.; Gómez-García, C. J.; Clemente, J. M.; Riou, A.; Molinie, P. *Inorg. Chem.* **2000**, *39*, 3771. (b) Vallejo, J.; Castro, I.; Déniz-Hernández, M. P.; Ruiz-Pérez, C.; Lloret, F.; Julve, M.; Ruiz-García, R.; Cano, J. *Inorg. Chem.* **2012**, *51*, 3289.
- (14) (a) Rochon, F. D.; Melanson, R.; Andruh, M. *Inorg. Chem.* **1996**, *35*, 6086. (b) Andruh, M.; Melanson, R.; Stager, C. V.; Rochon, F. D. *Inorg. Chim. Acta* **1996**, *309*. (c) Stanica, N.; Stager, C. V.; Cimpoesu, M.; Andruh, M. *Polyhedron* **1998**, *17*, 1787. (d) Vallejo, J.; Castro, I.; Cañadillas-Delgado, L.; Ruiz-Pérez, C.; Ferrando-Soria, J.; Ruiz-García, R.; Cano, J.; Lloret, F.; Julve, M. *Dalton Trans.* **2010**, *39*, 2350. (e) Vallejo, J.; Castro, I.; Ferrando-Soria, J.; Déniz-Hernández, M. P.; Ruiz-Pérez, C.; Lloret, F.; Julve, M.; Ruiz-García, R.; Cano, J. *Inorg. Chem.* **2011**, *50*, 2073.
- (15) (a) Ohba, M.; Tamaki, H.; Matsumoto, N.; Okawa, H. *Inorg. Chem.* **1993**, *32*, 5385. (b) Coronado, E.; Giménez, M. C.; Gómez-

García, C. J.; Romero, F. M. *Polyhedron* **2003**, *22*, 3115. (c) Marinescu, G.; Andruh, M.; Lescouëzec, R.; Muñoz, M. C.; Cano, J.; Lloret, F.; Julve, M. *New J. Chem.* **2000**, *24*, 527.

(16) (a) Muñoz, M. C.; Julve, M.; Lloret, F.; Faus, J.; Andruh, M. *J. Chem. Soc., Dalton Trans.* **1998**, 3125. (b) Rochon, F. D.; Massarweh, G. *Can. J. Chem.* **1999**, *77*, 2059.

(17) (a) Pardo, E.; Train, C.; Lescouëzec, R.; Boubekeur, K.; Ruiz, E.; Lloret, F.; Verdaguer, M. *Dalton Trans.* **2010**, *39*, 4951. (b) Coronado, E.; Galán-Mascarós, J. R.; Giménez-Saiz, C.; Gómez-García, C. J.; Ruiz-Pérez, C.; Triki, S. *Adv. Mater.* **1996**, *8*, 737. (c) Coronado, E.; Galán-Mascarós, J. R.; Giménez-Saiz, C.; Gómez-García, C. J.; Ruiz-Pérez, C. *Eur. J. Inorg. Chem.* **2003**, *12*, 2290. (d) Maxim, C.; Ferlay, S.; Train, C. *New J. Chem.* **2011**, *35*, 1254.

(18) (a) Kou, H.-Z.; Sato, O. *Inorg. Chem.* **2007**, *46*, 9513. (b) Coronado, E.; Galán-Mascarós, J. R.; Gómez-García, C.; Martí-Gastaldo, C. *Inorg. Chem.* **2005**, *44*, 6197. (c) Coronado, E.; Galán-Mascarós, J. R.; Martí-Gastaldo, C. *Polyhedron* **2007**, *26*, 2101. (d) Coronado, E.; Galán-Mascarós, J. R.; Martí-Gastaldo, C. *J. Am. Chem. Soc.* **2008**, *130*, 14987. (e) Coronado, E.; Galán-Mascarós, J. R.; Martí-Gastaldo, C. *CrystEngComm* **2009**, *11*, 2143.

(19) Kurtz, S. K.; Perry, T. T. *J. Appl. Phys.* **1968**, *39*, 3798.

(20) (a) Hooft, R. W. W. COLLECT; Nonius BV: Delft, The Netherlands, 1999. (b) Duisenberg, A. J. M.; Kroon-Batenburg, L. M. J.; Schreurs, A. M. M. *J. Appl. Crystallogr.* **2003**, *36*, 220 (EVALCCD).

(21) SADABS, version 2.03; Bruker AXS Inc.: Madison, WI, 2000.

(22) Sheldrick, G. M. SHELX97, *Programs for Crystal Structure Analysis (Release 97-2)*; Institut für Anorganische Chemie der Universität: Göttingen, Germany, 1998.

(23) Farrugia, L. J. *J. Appl. Crystallogr.* **1999**, *32*, 837 (WINGX).

(24) (a) Nardelli, M. *J. Appl. Crystallogr.* **1995**, *28*, 659. (b) Palmer, D. *CrystalMaker*; Cambridge University Technical Services: Cambridge, UK, 1996.

(25) (a) Homma, S.; Matsuda, H.; Ogita, N. *Prog. Theor. Phys.* **1986**, *75*, 1058. (b) Toma, L.; Lescouëzec, R.; Vaissermann, J.; Delgado, F. S.; Ruiz-Pérez, C.; Carrasco, R.; Cano, J.; Lloret, F.; Julve, M. *Chem.—Eur. J.* **2004**, *10*, 6130. (c) Ferrando-Soria, J.; Ruiz-García, R.; Cano, J.; Stiriba, S.-E.; Vallejo, J.; Castro, I.; Julve, M.; Lloret, F.; Amorós, P.; Pasán, J.; Ruiz-Pérez, C.; Journaux, Y.; Pardo, E. *Chem.—Eur. J.* **2012**, *18*, 1608. (d) Ferrando-Soria, J.; Grancha, T.; Julve, M.; Cano, J.; Lloret, F.; Journaux, Y.; Pasán, J.; Ruiz-Pérez, C.; Pardo, E. *Chem. Commun.* **2012**, *48*, 3539.

(26) (a) Lacroix, P. G.; Veret-Lemarinier, A. V.; Clement, R.; Nakatani, K.; Delaire, J. *J. Mater. Chem.* **1993**, *3*, 499. (b) Lacroix, P. G.; Clement, R.; Nakatani, K.; Zyss, J.; Ledoux, I. *Science* **1994**, *263*, 658. (c) Coradin, T.; Clement, R.; Lacroix, P. G.; Nakatani, K. *Chem. Mater.* **1996**, *8*, 2153. (d) Lagadic, I.; Lacroix, P.; Clement, R. *Chem. Mater.* **1997**, *9*, 2004. (e) Coradin, T.; Veber, M.; Francis, A. H.; Clement, R. *J. Mater. Chem.* **1998**, *8*, 1471.

(27) Cano, J. *VPMAG Package*; University of Valencia: Valencia, Spain, 2003.

(28) Lloret, F.; Julve, M.; Cano, J.; Ruiz-García, R.; Pardo, E. *Inorg. Chim. Acta* **2008**, *361*, 3432.

(29) Jakubas, R.; Ciunik, Z.; Bator, G. *Phys. Rev. B* **2003**, *67*, 024103.

(30) Gruselle, M.; Train, C.; Boubekeur, K.; Gredin, P.; Ovanesyan, N. *Coord. Chem. Rev.* **2006**, *250*, 2491.